Assessing Flood Risk Under Sea Level Rise and Extreme Sea Levels Scenarios Application to the Ebro Delta (Spain)

Sayol, J. M.; Marcos, M.

DOI
10.1002/2017JC013355

Publication date
2018

Document Version
Final published version

Published in
Journal of Geophysical Research: Oceans

Citation (APA)
Sayol, J. M., & Marcos, M. (2018). Assessing Flood Risk Under Sea Level Rise and Extreme Sea Levels Scenarios: Application to the Ebro Delta (Spain). *Journal of Geophysical Research: Oceans*, *123*(2), 794-811. https://doi.org/10.1002/2017JC013355

AGU PUBLICATIONS

JGR

Journal of Geophysical Research: Oceans

RESEARCH ARTICLE

10.1002/2017JC013355

Assessing Flood Risk Under Sea Level Rise and Extreme Sea Levels Scenarios: Application to the Ebro Delta (Spain)

J. M. Sayol[1,2] **and M. Marcos**[1,3]

[1]IMEDEA (UIB-CSIC), Esporles, Balearic Islands, Spain, [2]Now at TU Delft, Delft, the Netherlands, [3]Department of Physics, University of the Balearic Islands, Palma, Balearic Islands, Spain

Key Points:
- A new methodology for flood hazard assessment integrating mean sea level rise and extremes under climate change scenarios is presented
- Sea level rise includes seasonal and inter-annual variability, vertical land movements and joint extremes of storm surges and wind waves
- Offshore relative sea level rise is projected onshore by computing run-up in order to design flood hazard maps for Ebro Delta, Spain

Supporting Information:
- Supporting Information S1

Correspondence to:
J. M. Sayol,
J.M.SayolEspana@tudelft.nl

Citation:
Sayol, J. M., & Marcos, M. (2018). Assessing flood risk under sea level rise and extreme sea levels scenarios. application to the Ebro Delta (Spain). *Journal of Geophysical Research: Oceans*, *123*, 794–811. https://doi.org/10.1002/2017JC013355

Received 14 AUG 2017
Accepted 3 JAN 2018
Accepted article online 9 JAN 2018
Published online 1 FEB 2018

Abstract This study presents a novel methodology to estimate the impact of local sea level rise and extreme surges and waves in coastal areas under climate change scenarios. The methodology is applied to the Ebro Delta, a valuable and vulnerable low-lying wetland located in the northwestern Mediterranean Sea. Projections of local sea level accounting for all contributions to mean sea level changes, including thermal expansion, dynamic changes, fresh water addition and glacial isostatic adjustment, have been obtained from regionalized sea level projections during the 21st century. Particular attention has been paid to the uncertainties, which have been derived from the spread of the multi-model ensemble combined with seasonal/inter-annual sea level variability from local tide gauge observations. Besides vertical land movements have also been integrated to estimate local relative sea level rise. On the other hand, regional projections over the Mediterranean basin of storm surges and wind-waves have been used to evaluate changes in extreme events. The compound effects of surges and extreme waves have been quantified using their joint probability distributions. Finally, offshore sea level projections from extreme events superimposed to mean sea level have been propagated onto a high resolution digital elevation model of the study region in order to construct flood hazards maps for mid and end of the 21st century and under two different climate change scenarios. The effect of each contribution has been evaluated in terms of percentage of the area exposed to coastal hazards, which will help to design more efficient protection and adaptation measures.

1. Introduction

Sea level rise (SLR) is one of the most adverse consequences of global warming (Nicholls & Cazenave, 2010), posing one of the major threats for coastal regions. The Fifth Assessment Report (AR5) of the Intergovernmental Panel on Climate Change (IPCC) released in 2013 points out that sea level will continue to rise during the 21st century and beyond, regardless the socio-economic scenario considered (Church et al., 2013). Conversely, the magnitude of this rise will largely depend on the coastal site location and on the amount of greenhouse gases (GHG) emissions (Carson et al., 2016; Slangen et al., 2014, 2017). Despite few studies suggest that some natural systems such as small coral reef islands are more resilient to SLR (Kench et al., 2006, 2015), unceasing anthropization and SLR acceleration point toward an inescapable increasing risk of coastal hazards (Dangendorf et al., 2017).

The projected SLR due to increased GHG concentrations will submerge coastal low-lying areas and will also increase the exposure of the coasts to extreme events such as high storm surges and large ocean waves that cause sporadic floods. Although rare, those occasional inundations can be devastating, with negative environmental and economic impacts, especially for unprepared areas (Batstone et al., 2013). The combined effects of SLR and extreme marine events include the salinization of waters with the subsequent harming of crops and habitats, the damage of infrastructures or strong erosion favoring reshaping and, eventually, the loss of land (Brown et al., 2014). Additionally, all these processes are attenuated or intensified by vertical land movements, which are more important than SLR in some regions (Wöppelmann & Marcos, 2016). In particular, most of world deltas are facing higher subsidence rates than absolute SLR (Ericson et al., 2006; Syvitski et al., 2009), thus exacerbating coastal hazards.

Marine extreme events are the result of the combination of storm surges, tidal oscillations and ocean waves. We will focus on the Mediterranean Sea, a micro-tidal environment in which the concern of extreme events is associated to surges and waves extremes. The Mediterranean Sea is also the target of an extensive and

strong ocean modeling community (e.g., Ruti et al., 2016); in this context, we take advantage from the availability of a unique set of regional storm surge and waves with high spatio-temporal resolution that includes hindcast, control runs and climate scenarios of the 21st century.

All in all the present study integrates state-of-the-art information from ocean models with sea level observations in a novel workflow to provide the best possible assessment of mean SLR and marine extremes at local scale. Offshore information is then projected onto the coast by computing the wave run-up (Stockdon et al., 2006). Here feedbacks with river flow and sediments are not analyzed, as the priority is to solve long-term and extreme episodic sea level and wave variations. The accurate resolution of local climate forcing is critical, as it is an input for all subsequent steps such as modeling of coastal erosion, studies of socio-economic impacts, or the evaluation of other smaller-scale processes (Sánchez-Arcilla et al., 1996). The resulting information can be used to create flood hazard maps for vulnerable coastal sites. In this sense, the degree of vulnerability is directly related with the exposure to SLR, the probability of occurrence of an extreme event, and the risk of losing human lives, damaging key infrastructures or other economical (e.g., tourism, trading, fishing, . . .) and environmental impacts (Tessler et al., 2015). Additionally it is plausible to think that the range and sophistication of protection and adaptation measures to be implemented by stakeholders are strongly limited by the regional wealth. Therefore, it is expected that decision-makers will prioritize the adoption of contingency plans for the most sensitive sites. Among them are: populated coastal cities, harbors, beaches, deltas and biological reserves, to cite only a few. Coastal deltas are vulnerable regions that can be particularly exposed to experiment reshaping processes induced by SLR (e.g., Van De Lageweg & Slangen, 2017). Therefore the Ebro Delta, a muddy dominated delta located in the northwestern Mediterranean Sea, is considered an ideal site to apply the proposed methodology. With around 50% of its 320 km^2 below 0.5 m, it is an extremely vulnerable system with an intense anthropogenic pressure, a common characteristic of many other world deltas (Giosan et al., 2014).

A similar methodology combining mean SLR and extremes to the here proposed has been recently applied to the coast of Germany by Arns et al. (2017). However, to our knowledge this is the first time that the contribution of extremes has been solved in the Mediterranean Sea using high resolution projections and combining mean SLR, the joint effect of extremes and vertical land movements. Besides, this study extends and complements previous works already performed in the Ebro Delta that analyzed the risk of flooding under different relative sea level rise scenarios (e.g., Alvarado-Aguilar et al., 2012; Fatorić & Chelleri, 2012; Genua-Olmedo et al., 2016; Ibáñez et al., 2014; Jiménez et al., 1997, 2017; Sánchez-Arcilla et al., 1996, 1998, 2008), by considering mid-term sea level variability (seasonal and inter-annual) and a more accurate impact of extremes. To conclude, a range of uncertainties is given for sea level rise induced by extreme events.

The manuscript is organized as follows: section 2 describes extensively the methodology and data used; section 3 presents briefly the Ebro Delta; in section 4 flood hazard maps for Ebro Delta under climate change scenarios are presented; and finally section 5 includes a discussion of the obtained results and main conclusions of this study.

2. Study Area

With a subaerial surface of about 320 km^2 the Ebro Delta is one of the largest wetlands in the Mediterranean region. It is located in the northwestern Mediterranean Sea/northeastern Spanish coast (see Figure 1, bottom-right). It includes a National Natural Park with rich biodiversity hosting one of the largest populations of birds in Europe. Farming is at the core of the Ebro Delta economy with more than 75% of its area dedicated to agriculture, and 65% focused on rice production (Genua-Olmedo et al., 2016). Additionally it is a centre of several economic activities including the exploitation of salt marshes, fishing, hunting, and more recently aquaculture and tourism (Fatorić & Chelleri, 2012; Sánchez-Arcilla et al., 1996).

The abrupt decrease in Ebro River sediments discharge, with 99% less sediments than at the beginning of the 20th century (Rovira & Ibáñez, 2007), has reversed the growing trend of the Ebro Delta surface during the last centuries. The reason is the intensive construction of dams and water reservoirs. Presently there are more than 170 active dams in Ebro river basin, with 96% of water of Ebro River basin fully regulated (Jiménez et al., 2017). Thus, Ebro delta presents now a wave dominated coast with strong reshaping processes. As an example, eroded sediments from delta beaches have formed the north and south spits (see Figure 1) in the last 50 years indicating an intense longshore transport (Jiménez & Sánchez-Arcilla, 1993;

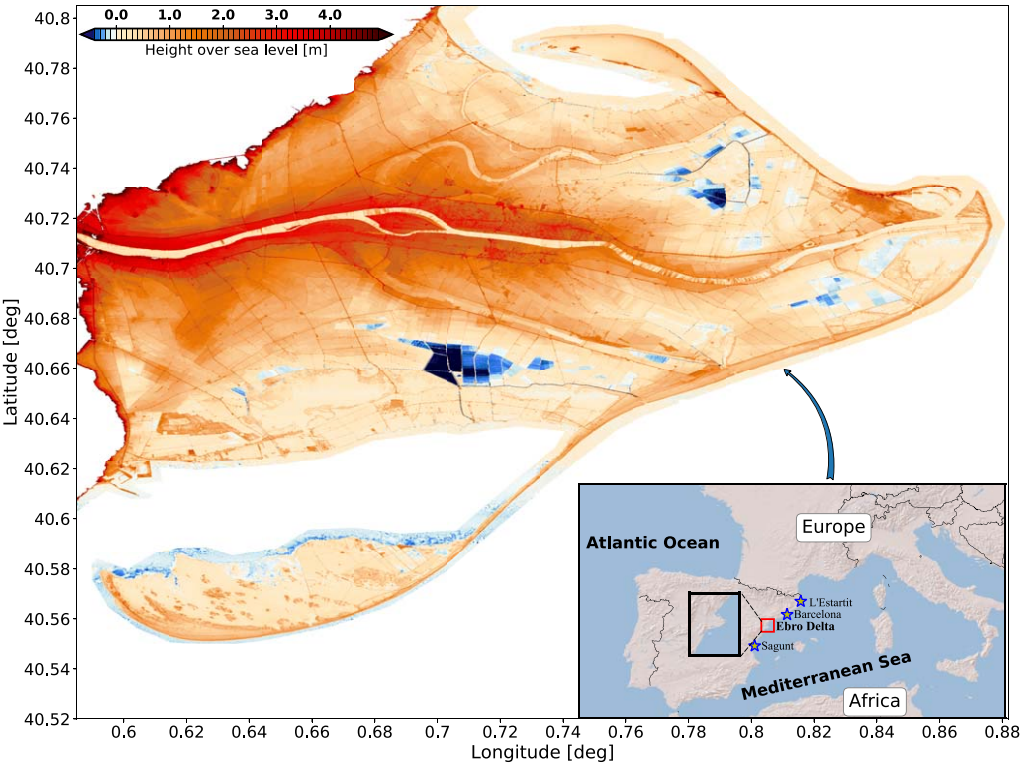

Figure 1. Topography of Ebro Delta (see background color, in meters). Additionally in the bottom right plot the Ebro Delta is positioned within the western Mediterranean Sea. The three blue stars near Ebro Delta indicate the position of tide gauges used to estimate seasonal and inter-annual amplitudes.

Jiménez et al., 1997). For a further description of Ebro Delta formation and evolution the reader is referred to, e.g., Maldonado (1972, 1986) and Sánchez-Arcilla et al. (1998).

The Ebro Delta is a suitable place to apply the methodology developed here since it shares common threats with other coastal regions and, more specifically, with other deltas (Ericson et al., 2006; Giosan et al., 2014). On one hand the lack of sediments is favoring land compaction resulting in a net subsidence average rate of about 3 mm/year, considering the mean of the last 20 years (Pipia et al., 2016). Besides, the projected construction of more dams and water reservoirs will likely aggravate the land sinking process. On the other hand, mean SLR in the Mediterranean Sea is accelerating in the last decades with a trend about 2.6 $\pm$ 0.2 mm/year since 1993 (Marcos et al., 2016). Overall it makes the Ebro Delta a vulnerable place with high risk of surface loss and saltwater intrusion, and exposed to mid and long-term negative environmental, social and economic impacts.

3. Data and Methods

3.1. Local Mean Sea Level Rise With Uncertainties

Yearly mean SLR for the area of interest is obtained from the last global IPCC projections (Church et al., 2013), available through the Integrated Climate Data Centre website hosted at the University of Hamburg (http://icdc.cen.uni-hamburg.de/1/daten/ocean/ar5-slr.html). These mean SLR projections consist of gridded 1°x1° sea surface height (SSH) fields that include the following contributors: ocean dynamical changes, global ocean thermal expansion, inverted barometer effect, melting land ice from Greenland, Antarctica and glaciers, changes in land water storage and glacial isostatic adjustment (GIA). Projected changes in the different mean SLR components are referred to the average of the period 1985–2005. Projections are available for Representative Concentration Pathways (RCP), RCP4.5 and RCP8.5 climate change scenarios. Together with the ensemble average of each component also the multi-model ensemble spread is provided in the form of 5% and 95% confidence intervals.

To assess local mean SLR from global maps, we have selected the time series corresponding to the closest grid point of each component to the study area (~1 km off the Ebro Delta coast), except for the ocean dynamics contributor. In this case, the low spatial resolution of the ocean models used to derive the projections does not represent correctly the exchanges through the Strait of Gibraltar and prevents from using the SSH fields in the Mediterranean Sea and any other marginal sea. Nevertheless, since at basin scale and in the long term the Mediterranean sea level follows sea level changes in the nearby Atlantic Ocean (Jordà & Gomis, 2013), we have thus extracted the time series averaged over the region of the Gulf of Cadiz and taken them as representative of basin averaged ocean dynamical projections. The results are not sensitive to the area chosen as far as it remains within the vicinity of Gibraltar. Uncertainties in the different components have been combined as in Church et al. (2013).

The multi-model ensemble mean averages out internal model variability which means that it lacks seasonal and inter-annual variability that contribute to higher/lower mean sea levels. We have accounted for this variability as part of the uncertainties in the mean sea level projections. Seasonal and inter-annual variability have been quantified on the basis of three in-situ tide gauges located close to the area of study (see stars in the inset of Figure 1), namely L'Estartit (operated during the period 1 January 1989 to 1 January 2015), Sagunt (1 January 2007 to 1 January 2014) and Barcelona (1 January 1993 to 1 January 2014). Monthly tide gauge records were downloaded from the Permanent Service for Mean Sea Level (PSMSL) website (Holgate et al., 2013). Original time series have been detrended. The seasonal signal has been extracted as the sum of the annual and semiannual Fourier terms of detrended tide gauge records, whereas the inter-annual signal has been computed using a low-pass Lowess filter with a time span of 360 days. Seasonal and inter-annual signals in this region are uncorrelated to each other, shown by the distribution of correlations obtained using a random-phase perturbation (Ebisuzaki, 1997) (supporting information Figure S2). Therefore, the uncertainty introduced by this variability has been computed as the linear sum of the annual amplitude seasonal signal and the standard deviation of inter-annual time series. This uncertainty has been finally added to that provided by the multi-model ensemble spread. The linear addition of both signals is justified because we seek the maximum impact of natural variability for a given period.

3.2. Extreme Events

Marine extreme events arise from the interplay of surges, waves and astronomical tides. We neglect the latter as tides are a small contributor in the Mediterranean Sea with values of the M_2 constituent of about 5 cm in most of the basin (Tsimplis et al., 1995) and we thus consider only surges and waves. Numerical simulations of storm surges over the Mediterranean Sea during the 21st century have been used to evaluate changes in the extreme surges. These simulations are the same as those described in Marcos et al. (2011) and consist of a hindcast run for the periods 1958–2001, a historical run forced with observed greenhouse gases concentrations (1950–2000) and three projections under B1, A1B and B2 climate change scenarios for the period 2001–2100. For completeness their characteristics are summarized here, although more details can be found in Marcos et al. (2011) and Jordà et al. (2012). Numerical simulations are conducted using the HAMSOM model (Backhaus, 1985) in its barotropic version, run over the Mediterranean Sea with a spatial resolution of $^1/_{4^\circ}$ in latitude and $^1/_{6^\circ}$ in longitude and forced with 6 hourly dynamically downscaled surface (10 m) atmospheric pressure and wind fields provided by ARPEGE-v3 climate model (Déqué & Piedelievre, 1995). The same wind forcing fields were used to generate wind-waves simulations with the numerical model WAM (WAMDI Group, 1988) run over the Western Mediterranean basin with a spatial resolution of $^1/_{6^\circ}$. As in the case of surges, the same set of simulations and for the same periods were carried out, including a hindcast, a historical run and three climate change scenarios. More details on the model setup and forcing can be found in Martínez-Asensio et al. (2013). Altogether a set of surge and waves simulations, consistent to each other, have been used.

The probability of reaching a determined flood level tends to be higher (or the return period smaller) when surges and waves are correlated. In that case, if return periods of surges and waves are derived independently they will tend to be overestimated, thus underestimating the real risk. On this basis, our methodology takes into account that surge and significant wave height (H_s) series can be significantly correlated, resulting in an exacerbation of the return level (RL) or, equivalently, in a reduction of the return period. Results from Wahl and Chambers (2014) in the US coasts suggest that an indicative (although nonconclusive) rule is that the relationship between surge and H_s is significant at 90% level for Kendall correlations > 0.2. This value is also confirmed in the case study after visual inspection of the simultaneous surge and wave extremes. Hence, for correlated variables it is more appropriate to compute the joint return

period. Hawkes et al. (2002) reviewed some methods to estimate the joint return period, mostly based on the Monte Carlo simulation of design states of waves and water levels. Here we apply the theory of copulas (Coles, 2001; Sklar, 1959), that have become very popular in recent years in climate studies, although they have been used for long time. Copulas aim to reproduce the statistical structure of dependence between two or more variables departing from best fitted univariate marginal distributions of probability. In particular, the relationship between an n-variate cumulative distribution function and a copula is defined as:

$$F_{X_{1,2,\ldots,n}}(x_1, x_2, \ldots, x_n) = C[F_{X_1}(x_1)F_{X_2}(x_2), \ldots, F_{X_n}(x_n)], \quad (1)$$

where C is the copula function that depends on the univariate marginal cumulative distributions $F_{X_n}(x_n)$, being x_n uniformly distributed random variables.

Previous studies have used copulas to characterize rainfall/drought intensity and duration (e.g., De Michele & Salvadori, 2003; Shiau, 2006), river and snow-melt flooding (e.g., Ozga-Zielinski et al., 2016; Reddy & Ganguli, 2012), extreme waves (de Waal and Van Gelder, 2005), sea storms (De Michele et al., 2007) and also for the combination of surges and H_s (e.g., Arns et al., 2017; Rueda et al., 2016). There are several families of copulas in the literature, being the most used the Archimedean and elliptical ones, or a combination of them (for a more complete description of types of copulas the reader is referred to Nelsen (2006) and Salvadori et al. (2007)). One of the benefits of using copulas is that the joint return period is simply defined by the copula itself and the time resolution of the data (Salvadori et al., 2011).

For the sake of clarity, the step by step description of the procedure followed to get the joint return period of surges and H_s via copulas is described below:

a. *Selection of independent events*. To avoid biased return levels only the independent relative maxima of surges are included in the analysis. The highest values of H_s and wave peak period (T_p) within $\pm$6 hours of the maximum surge are also retained to build the set of triads of (surge, H_s, T_p). Independency between events depends on the size and translation velocity of storms, but a typical value of 72 hours is accepted for the Mediterranean Sea region (Marcos et al., 2009).
b. *Selection of extreme events*. Extreme events have been selected following the Peak Over Threshold (POT) approach (Davison & Smith, 1990). Only those triads of independent events of (surge, H_s, T_p) whose values of surge are over a predefined threshold are retained. This threshold must be chosen to, on the one hand, provide a number of events large enough to ensure statistical robustness and, on the other, to represent actual extreme events. In order to find a well suited threshold many sensitivity tests can be performed (Coles, 2001). In this work the threshold was chosen intending to balance a significant Kendall correlation at 95% of significance level with the selection of "true" extremes. To maintain the comparability between different models and scenarios the percentile 96th was applied for all cases. In practice, it means that the same number of data is employed, about 4 ($\sim$3.8) extremes per year on average, for all simulations. It is worth to notice that the Block Maxima approach can also be applied, which consists on selecting a fixed number of maxima per block of time, usually a year (see e.g., Kotz & Nadarajah, 2000). However, caution is advised in this case since in the Mediterranean Sea extreme events occur predominantly on late fall, winter and early spring and consequently grouping events in a calendar year basis may add a bias.
c. *Fitting of univariate marginal distributions*. The extreme surge and H_s series are fitted separately to a set of parametric statistical distributions that include Generalized Pareto Distribution, Weibull, gamma, log-normal and exponential distributions. Except for the exponential distribution, simpler with only one parameter to fit, all other distributions have two. The distribution that fits the data with the maximum likelihood is selected for each case. Additionally, the Root Mean Square Error (RMSE) between all five theoretical curves and the empirical cumulative distributions was estimated to confirm the agreement with the maximum likelihood criterion. The possibility to generate new synthetic data from the selected statistical distributions will be used in the next subsections to compute the joint return period through copulas. A further description of the tested statistical distributions is presented in the Supplementary Material.
d. *Selection of best fitted copula*. By making use of the above estimated univariate marginal distributions of surges and H_s, copulas are computed among the Archimedean and elliptical copulas. More specifically the following theoretical copulas were tested: Frank, Clayton, Gumbel, Normal and t-Student (see mathematical expressions in the Supplementary Material). Copulas are fitted through a maximum likelihood procedure. From previous works there are several ways to proceed to check the goodness-of-fit, although none of them is completely conclusive. One approach is to estimate the RMSE between the empirical

copula and each fitted copula or, similarly, directly to compare all copula maximum likelihood estimators to get the best fitted. Additional goodness-of-fit estimators such as the Bayesian, Akaike or Cramér-von Mises information criteria are also found in the literature. In this work it has been used the comparison of the joint nonexceedance distribution of empirical and fitted copulas by means of the RMSE, as in Wahl et al. (2012). For example, for the bi-variate case the empirical joint nonexceedance probability is expressed as (Gringorten, 1963):

$$F_{UV}(u_i, v_i) = P(U \leq u_i, V \leq v_i) = \frac{\sum_{j=1}^{i} \sum_{k=1}^{i} N_{jk} - 0.44}{N + 0.12}, \quad (2)$$

where the pairs (u_j, v_k) refer to surge and H_s in this work and are organized in ascending order in relation to u_j. N_{jk} is the number of occurrences of (u_j, v_k), with $u_j < u_i$ and $v_k < v_i$, $i = 1, \ldots, N$ and $1 \leq j, k \leq i$. Additionally a Q-Q plot of theoretical versus empirical joint nonexceedance distributions and a Kolmogorov-Smirnov test (K-S test) to check vertical separation have been applied.

e. *Joint return period and return levels*. Salvadori et al. (2011) summarized different possibilities to define the joint return period. In this work it is preferred to use the "OR" joint return period, i.e., the expected time to record a value either of surge or H_s exceeding a given threshold. Mathematically, this is expressed as:

$$P(U > u \cup V > v) = 1 - F_{UV}(u, v) = 1 - C[F_U(u), F_V(v)], \quad (3)$$

being the return period inversely proportional to equation (3). Thus, different values of C can proceed from several combinations of surge and H_s. However, each C is related unequivocally to a determined return period. Besides, the corresponding T_p for each value of H_s has been obtained from a linear fit between the independent extreme events of T_p against H_s, as in Arns et al. (2017).

Among the different combinations of surge, and H_s defined by a certain value of C (or a return period), three sets that cover a wide range of sea levels induced by extreme events are selected. In particular, those values representing percentile 99, percentile 50 (median) and percentile 1 of the total sea level generated by the joint effect of surge and wave run-up. Thus, an interval of uncertainty accounting for the impact of extremes is built, given that different combinations may have a distinct effect on flooding levels depending on the topographic features of the study area. The equation of wave run-up employed here was deduced empirically by Stockdon et al. (2006), equation (19) therein, and depends on H_s, T_p, land slope (β) and surge, which determines the set-up. This expression accounts for the 2% of highest levels. The accessibility to a very high resolution bathymetry/topography of the area of study is thus critical for an accurate estimation of the land slope and consequently of the run-up term.

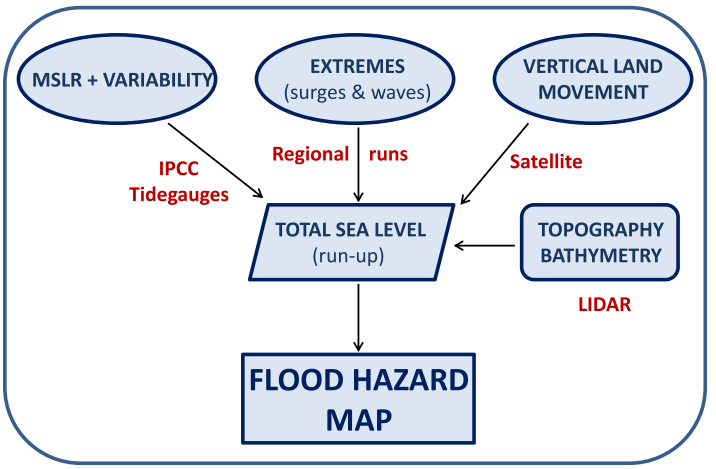

Figure 2. Workflow of the methodology. Mean Sea Level Rise (MSLR), extreme events due to the joint effect of storm surges and wave extremes, and vertical land movements are all together integrated and projected onshore through computing the wave run-up, to construct coastal flooding hazard maps. The accuracy of these maps will depend on the spatial resolution of available topography/bathymetry for the area of study. As an example, the methodology will be applied for Ebro Delta for mid and late 21st century, considering socio-economic scenarios RCP4.5 and RCP8.5, and a return period of 10 years.

On this point we would like to mention that another manner to estimate return levels is to compute the tri-dimensional copula of surges, H_s and T_p. By doing so more combinations of surge, H_s and T_p arise to give a certain water level because now T_p can take any value within the range of T_p provided by the independent events. However, this apparent positive side involves also an important drawback because some of those new combinations, despite being statistically consistent, are sometimes physically unrealistic, with simultaneous values of exceedingly small H_s and long T_p(see supporting information Table S1). Therefore we have preferred to estimate the bi-variate copula of surges and H_s and to obtain directly T_p from a linear fit against H_s. For completeness a comparison of both methods is presented in the Supplementary Material (supporting information Figures S8–S10 and Table S1) with overall similar results in terms of percentage of flooded area with values falling within the uncertainty range.

The whole procedure is repeated for each available numerical model (M) and simulations -either hindcast (H), control (Ctrl) or scenario (S)-. To estimate the return level (RL), 30 year blocks have been used. Changes in RLs have been computed as the difference between RLs in scenarios (2030–2060 for mid-century and 2070–2100 for late

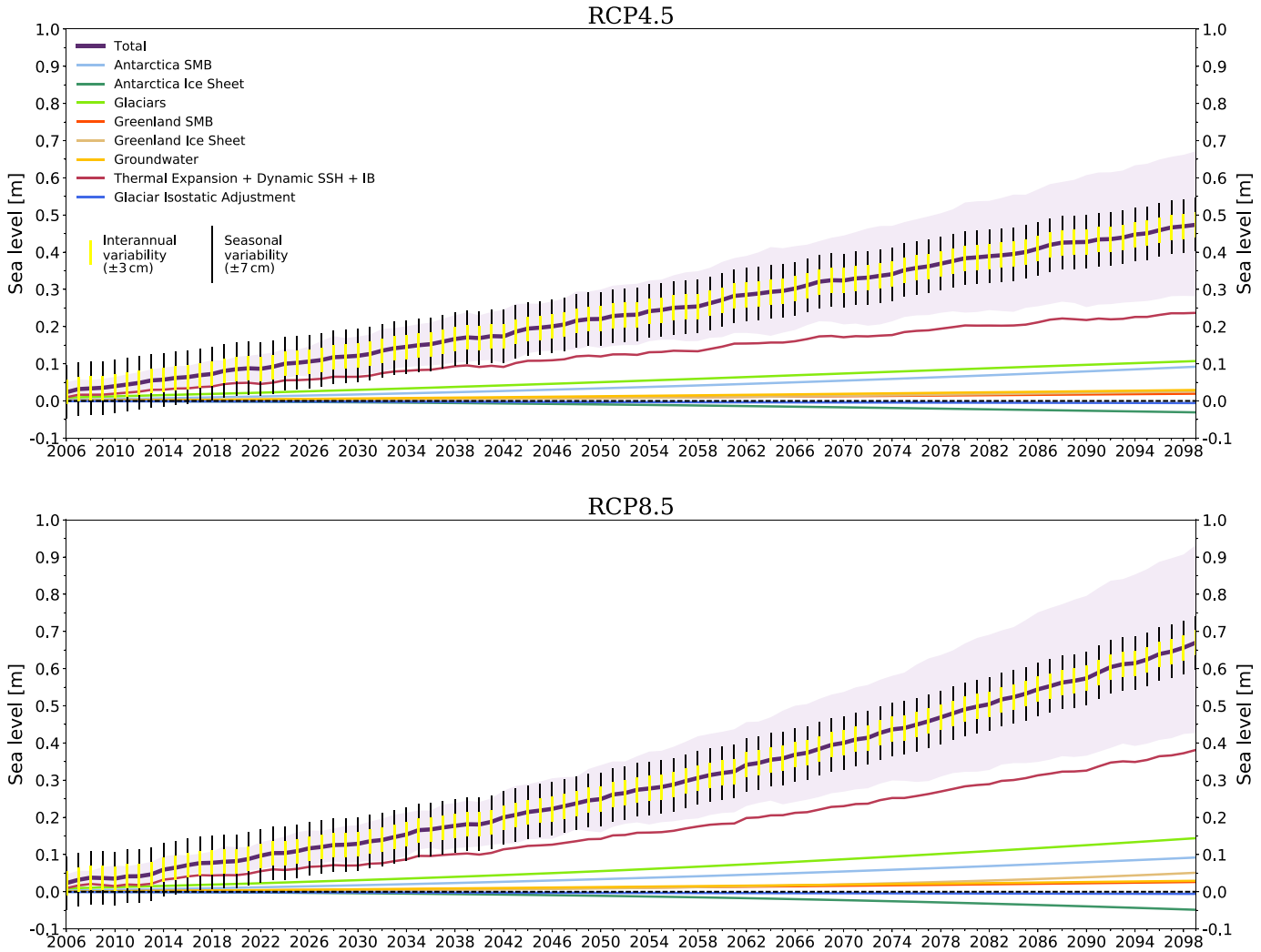

Figure 3. Yearly mean Sea Level Rise (SLR, solid thick dark purple line) from the ensemble average of AOGCMs at the nearest Ebro Delta grid point (in meters). Time series cover the period 2006–2099. Results for two socio-economic scenarios are showed: (top) RCP4.5 and (bottom) RCP8.5. Light purple shading area represents 5–95% mean SLR interval of confidence. All sea level components are plotted separately with thinner solid lines of different colors. The component that refers to thermal expansion + dynamic SSH + inverted barometer has been obtained averaging several grid points located in the left side of the Strait of Gibraltar (see section 2.1 for further explanations). Seasonal and inter-annual sea level variability has been estimated from in situ tide gauges (see section 2.1 and Figure 4), being indicated by vertical solid lines (black and yellow colors respectively).

century) and Ctrl (1970–2000) runs. Then, the absolute RL is estimated by adding this difference to the RL from the hindcast (computed using the period 1970–2000), which is taken as the best representation of present-day climate. This can be expressed as follows:

$$RL_{M,S,T}(\text{surge}, H_s) = RL_{M,H}(\text{surge}, H_s) + RL_{M,S,T}(\text{surge}, H_s) - RL_{M,Ctrl}(\text{surge}, H_s) \quad (4)$$

where the dependence of return levels on the pair selected -the most probable obtained with copula- of surges and significant wave height (surge, H_s), has been stated explicitly. The period of the RL has been established in 10 years, a moderate value that ensures that RL correspond to real extremes (only about 3 events in the 30 year blocks) but at the same time probable enough to be a real threat in a short time frame.

3.3. Vertical Land Movement

Vertical land motion (VLM) of the Earth's crust can, at some particular locations, reach values comparable to those of absolute mean SLR. This is the case of many world deltas (Ericson et al., 2006; Syvitski et al.,

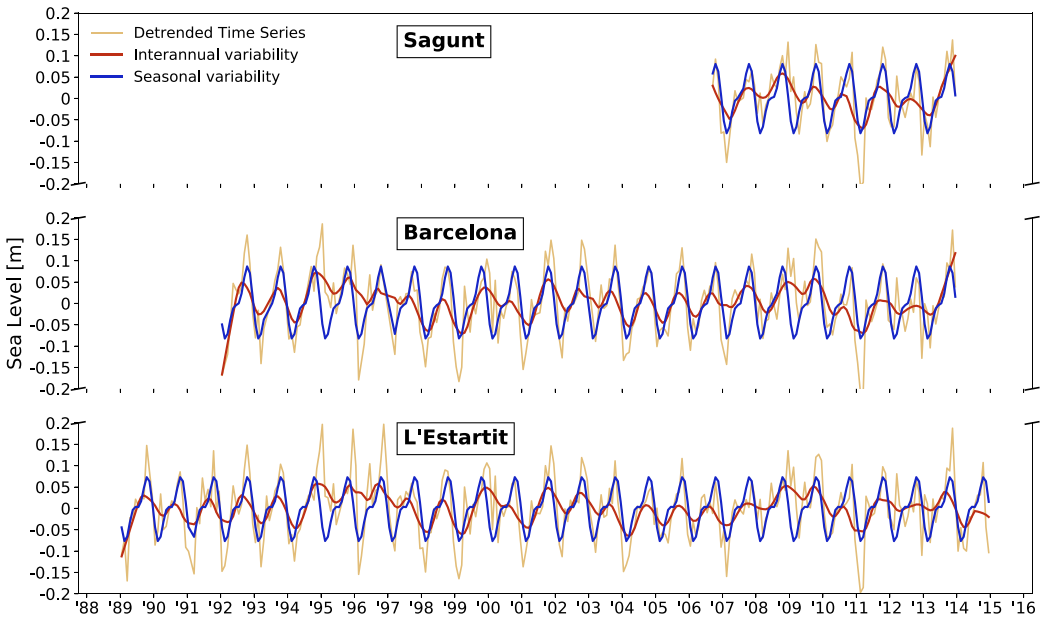

Figure 4. Sea level measured by three tide gauges located near Ebro Delta (unit in meters, for exact locations see blue stars in Figure 1). Original time series have been linearly detrended. Blue lines represent the seasonal variability, estimated as the combination of annual and semiannual Fourier terms. In red color it is shown the inter-annual signal resulting from the application of a Lowess low-pass filter with a span of 360 days.

2009), in which VLM exacerbates the risk of coastal flooding. Previous studies that analyzed potential impacts of SLR on Ebro Delta applied an indirect rate of subsidence estimated through sediment balance (Sánchez-Arcilla et al., 1993), with a value of 3 mm/year. This number has been recently confirmed with satellite data by Pipia et al. (2016) using remote sensing observations between years 1992 and 2011. It must be noted, however, that this is an average value but there is a large variability of VLM across the delta plain, with rates ranging between 2 and 8 mm/year. For the purpose of this work and in absence of detailed projections of VLM it will be assumed a stationary and homogeneous rate of subsidence of 3 mm/y during the 21st century over the entire delta.

3.4. Total Relative Sea Level

Total relative sea level at the coast has been computed to account for all the terms described above, which can be expressed as:

$$\mathrm{TSLR} = \mathrm{mean\ SLR} + \mathrm{Vertical\ Land\ Movement} + \mathrm{wave\ run{-}up}\left(H_s, T_p, \beta, \mathrm{surge}\right) \quad (5)$$

where wave run-up is computed with the empirical expression of Stockdon et al. (2006).

Total relative sea level has been estimated for each scenario, return period and series of triads of (surge, H_s, T_p) considering the predicted mean SLR, its uncertainty (including seasonal and inter-annual variability) and the VLM.

3.5. Flood Hazard Maps

The final step of the methodology is to provide maps of flood risk by inundating the high resolution topography according to the values of total relative sea level for mid and late 21st century (see Figure 2). These flood hazard maps indicate flooded areas incorporating the projected percentage of area inundated. A permanently inundated area will result from mean SLR plus delta subsidence, whereas a temporary inundated area has been defined as that exposed to moderate (10 year RL) extreme events. For simplicity flooded areas include all those grid points below projected sea level without taking into account if the inundated regions are directly connected to the sea. However, a test for a value of mean SLR of 0.12 m demonstrates that the flooded area is overestimated in less than 0.5% when this approach is used. This quantity increases to 5% for a mean SLR of 0.5 m, and up to 8% for 0.9 m, enough for the purpose of this

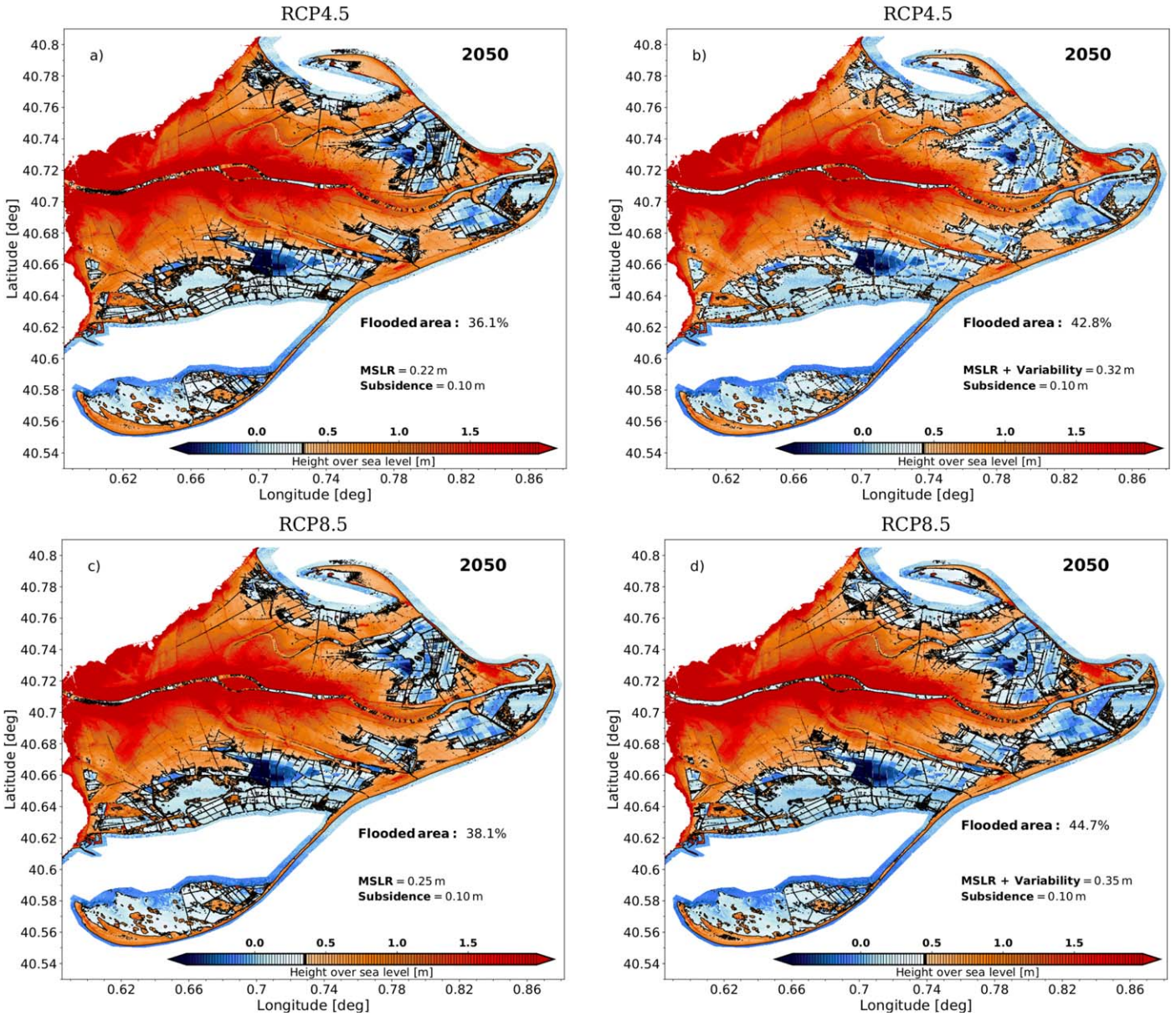

Figure 5. Flood hazard maps for mid 21st century and for (top) RCP4.5and (bottom) RCP8.5 scenarios. All four plots include the impact of mean SLR (0.22 m for RCP4.5 and 0.25 cm for RCP8.5) between 2006 and 2050. Subsidence is also included in all plots (estimated as 0.1 m in 2050 respect the year 2016). The impact of adding seasonal and inter-annual variability is shown in the right plots (seasonal + inter-annual uncertainties = 0.1 m). The thick vertical black line in the colorbar separates inundated areas (blue tones) from those dry (red tones).

study, as our interest here is to solve accurately the climatic forcing and to compare the relative contribution of each term to SLR.

4. Results

4.1. Flooding of Ebro Delta Due to Mean SLR (With Uncertainties) and Land Subsidence

The risk of permanent flooding depends highly on the net result of local mean SLR and vertical land movements. In the case of Ebro Delta the existence of a rate of subsidence implies that both effects act to favor land flooding with the subsequent potential loss of wetland.

Yearly mean SLR -total and individual components- for the 21st century at the Ebro Delta under RCP4.5 and RCP8.5 are presented in Figure 3. All curves are referred to the average of the period 1985–2005 and span

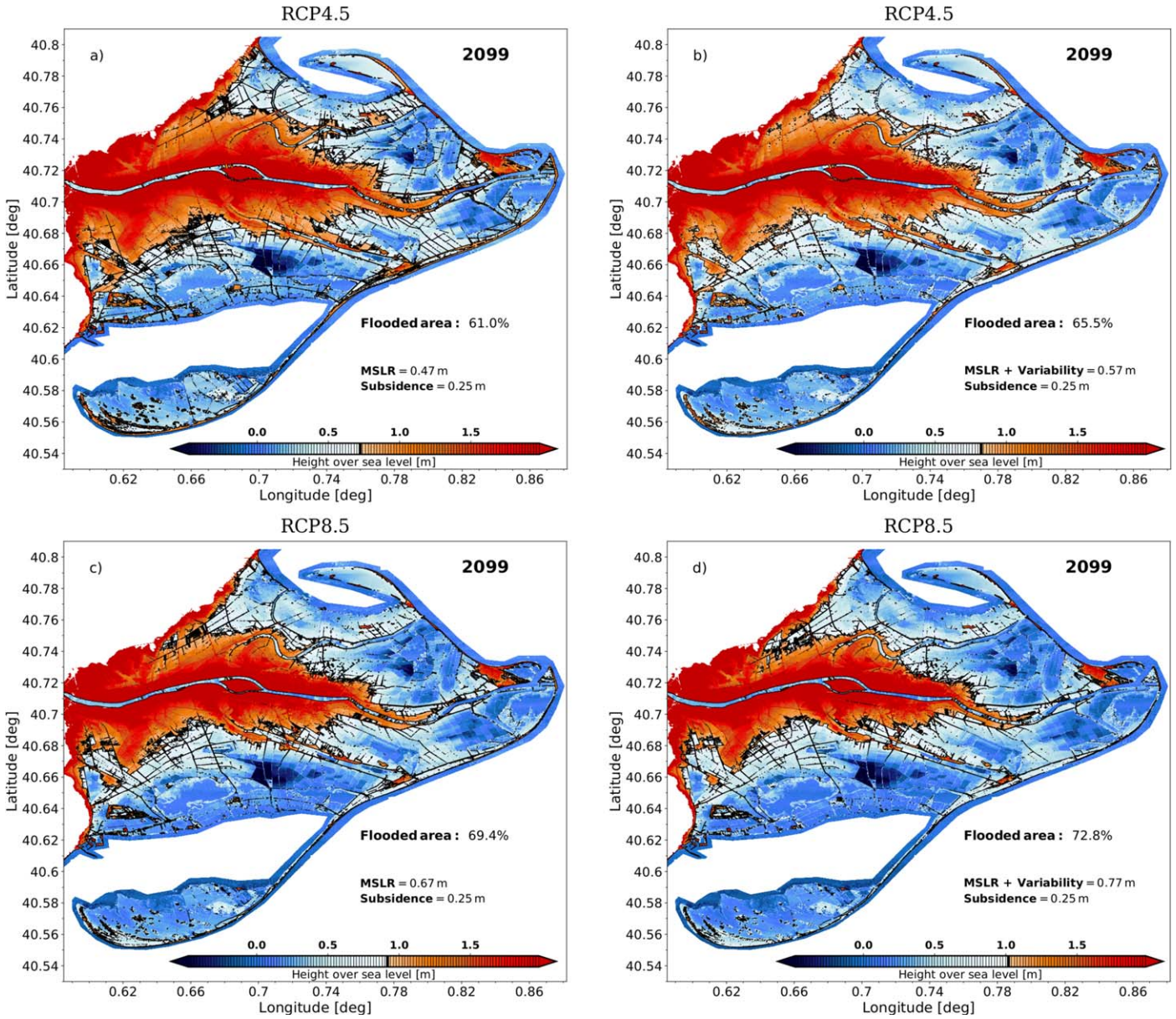

Figure 6. Same as Figure 5 but for end of 21st century. In this case mean SLR is 0.47 m for RCP4.5 and 0.67 m for RCP8.5. Subsidence is 0.25 m for all plots. Variability of 0.1 m has also been added in the right plots.

the period 2006–2099. Light purple shaded area indicates 5–95% confidence interval for mean SLR, estimated according to the methodology developed in Church et al. (2013). A comparison between time series of both scenarios suggests a similar behavior of mean SLR until 2050, with an increase of 0.22 m for RCP4.5 and of 0.25 m for RCP8.5. Since mid-century mean SLR in both scenarios diverges and the increases by 2099 are 0.47 m for RCP4.5, and 0.67 m for RCP8.5.

Monthly sea level records measured by three tide gauges nearby the Ebro Delta are presented in Figure 4. Seasonal and inter-annual signals are represented separately for each record. Despite the temporal coverage differs largely among tide gauges, ranging between 7 years for Sagunt and 25 years for L'Estartit, seasonal and inter-annual amplitudes are similar at all sites. In particular, the amplitude of the seasonal signal has been estimated in 7 cm while that of the inter-annual signal is 3 cm. Independence between seasonal and inter-annual signals has been verified at zero time-lag using the random-phase method (Ebisuzaki,

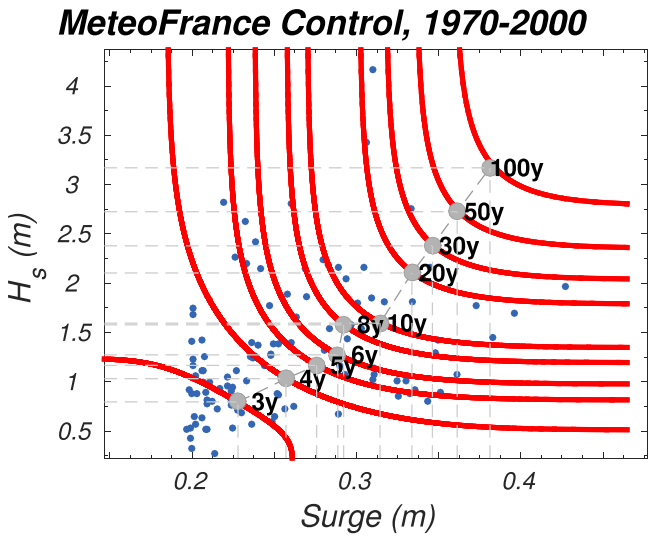

Figure 7. Copula-based joint contours of probability of surges and significant wave height (H_s) for MeteoFrance control simulation. The period covered is 1970–2000. Red contours correspond to pairs of surge and H_s with equal return period. Blue dots indicate independent extreme events over percentile 96th, as described in section 2.2. Gray dots indicate the most probable pair of surge and H_s according to the maximum PDF after the addition of individual PDFs of surge and H_s.

1997). For a further description of the method the reader is referred to the Supplementary Material (supporting information Figures S1 and S2). Given that both signals are independent, their uncertainties can be linearly combined and are represented in Figure 3 (solid black and yellow vertical lines). A comparison between the amplitudes and the vertical width of the shaded region shows that, until 2060, the ensemble mean uncertainty is of the order of seasonal and inter-annual amplitudes; conversely, after 2060 ensemble uncertainties dominate over seasonal and inter-annual signals.

Flooded area resulting from mean SLR and subsidence is represented for mid and end of the 21st century in Figures 5 and 6, respectively. All maps incorporate mean SLR and subsidence for scenarios RCP4.5 (top plots) and RCP8.5 (bottom plots). Additionally, a worst case scenario is built by including the effect of natural variability acting with a positive sign, that is, by assuming that in the chosen period the seasonal and inter-annual variability acts by increasing the mean SLR. The impact of adding seasonal and inter-annual variations is presented in the right plots of Figures 5 and 6. To facilitate comparisons the percentage of the area of Ebro Delta flooded is provided inside each plot in bold numbers and ranges between 36% and 45% in 2050 and 61% and 73% by the end of the century.

Due to the accelerated mean SLR linked to higher GHG concentrations, the flooded area is larger for RCP8.5 than for RCP4.5 scenario, with about 2% more for year 2050 and around 7–8% for 2099. Conversely, the effect of adding variability (which amounts to 0.1 m) is greater in 2050, with an increase of around 6–7% of the area submerged in both scenarios, while the impact for 2099 amounts to 3–4%. This result obeys the topography of Ebro delta, where more than 50% of its area is below 50 cm above sea level and about 70% is below 1 m (Alvarado-Aguilar et al., 2012). Maps without the contribution of land subsidence are available in the Supplementary Material (supporting information Figures S6 and S7).

4.2. Flooding of Ebro Delta in Response to Mean SLR and Extreme Events

Areas at risk of temporary flooding due to their exposure to extreme marine events as sea level rises, have been estimated by computing the return levels of the compound projected surges and waves, superimposed to mean sea level projections.

Figure 7 shows one example of joint contours of probability computed via copulas. Blue dots identify those pairs of independent events of simulated (surge, H_s) over 96th percentile used for fitting copulas and the set of return levels for fixed return periods is depicted with solid red contours. The most probable pair of surge and significant wave height for each return period is highlighted with a gray circle. The example in Figure 7 is based on data from the MeteoFrance Control run, covering from July 1969 to June 2000 (see supporting information Table S1). Supporting information Table S1 provides the most probable pairs of surge and H_s for all simulations and for a return period of 10 years. In the same table, the selected pairs used for constructing flood maps are highlighted in bold. For coherence with previous results and given the similarities between their gases concentrations, A1B scenario (Aemet Hadley) has been associated with RCP4.5 and A2 (MeteoFrance) with RCP8.5. The selected values of H_s (and T_p) and surge are also used to estimate total relative sea level through equation (5), including the run-up computation (i.e., also accounting for set-up and swash terms). To compute the run-up term, the slope (β) of the local topography is needed. The slope (β) has been evaluated at each grid point taking the shortest distance between that point and the closest watered point. The more accurate the set-up, the more correct local relative sea level can be estimated.

The results of the impact of extreme events have been mapped in Figures 8 and 9 for those combinations of surge, H_s and T_p corresponding to percentile 99 (all cases are described in supporting information Table S1, LF (linear fit) method). These flooding maps now include the areas submerged due to mean SLR

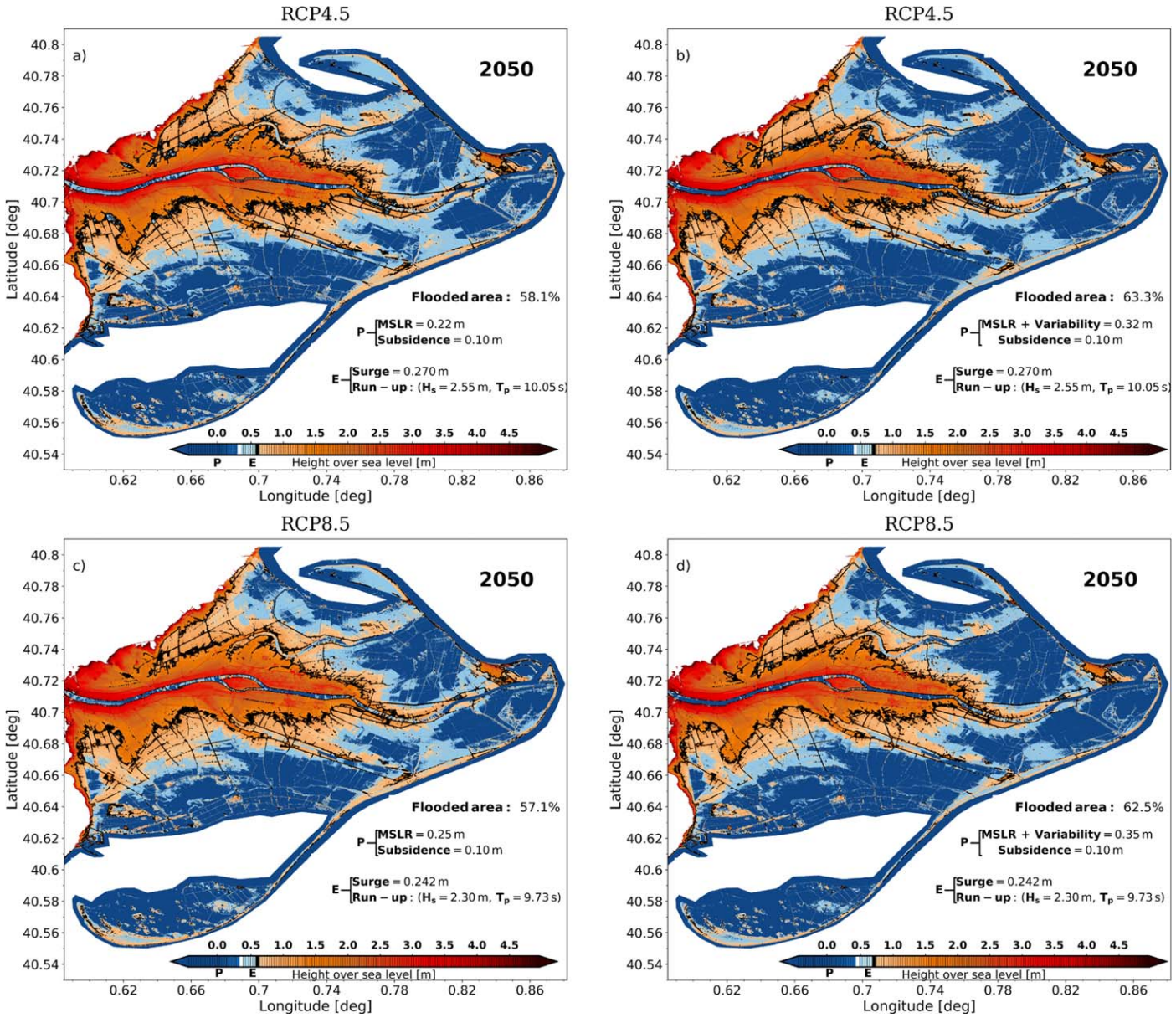

Figure 8. Flood hazard maps including extremes for mid 21st century. Top and bottom plots correspond to scenarios RCP4.5 and RCP8.5, respectively. P and E refer to permanent (dark blue background color) and extremes (light blue background color) terms of land inundation (including the permanent flooding shown in Figures 5 and 6 plus the effect of surge and waves through run-up). As in previous figures, right plots include in the permanent term the impact of a positive variability.

as well as the areas exposed to a surge-wave 10 year return level. Given the large range of possible values, particular cases have been selected to illustrate the results, whose information is labeled in the inset of each map. The overall results are further summarized in Figure 10, where hash lines in the top of the bars account for the uncertainty of extremes from percentile 1, percentile 50 and percentile 99 combinations Results for year 2050 and RCP4.5 for percentile 99 (Figure 8, top) show that the percentage of area flooded is 58.1% when the ensemble average mean SLR is used and it is 5.2% higher when variability is included, reaching 63.3%.The percentage of area flooded for scenario RCP8.5 (Figure 8, bottom) oscillates between 57.1% and 62.5%. Interestingly, the combination of surge and waves corresponding to percentile 99 does not always provide the maximum flooding (compare these results with percentages denoted by the hash area in Figure 10). The reason is that ultimately it depends strongly on the topographic features. For

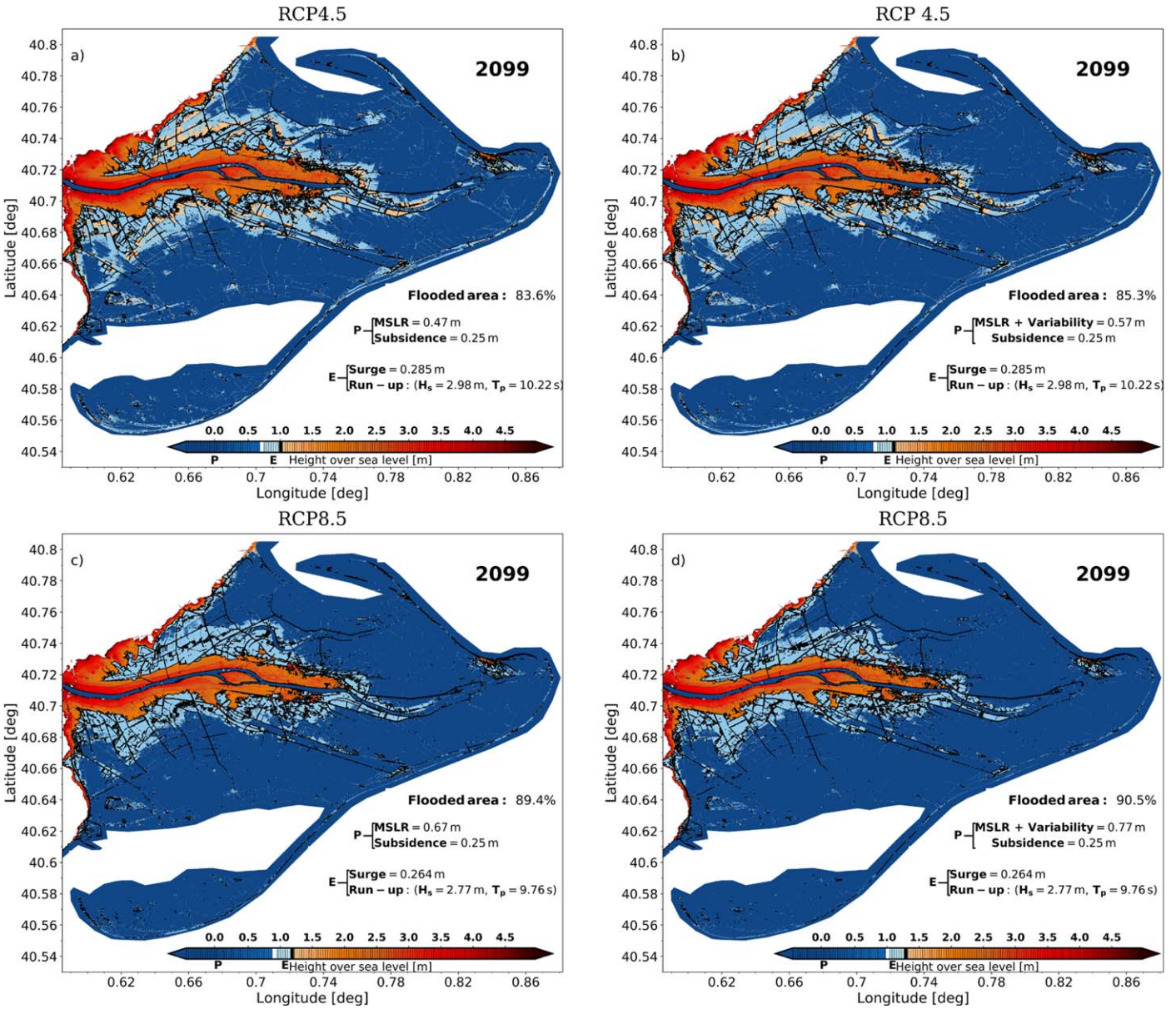

Figure 9. Same as Figure 8 but for year 2099.

instance, depending on land slope and configuration, flooding by a small surge can be larger than that of a relatively big wave (or vice versa). This fact supports the need for a range of uncertainties to cover the effect of different combinations. Additionally the submersion is greater for RCP8.5 due to a higher mean SLR, but the impact of extremes is larger for scenario RCP4.5.

The previous result for mid 21st century turns out to be the opposite for the end of the century (Figure 9). The reason is that, although extremes are very similar, the projected mean SLR is significantly higher for RCP8.5 than for RCP4.5 (0.67 m versus 0.47 m) by the end of the century. This yields finally a significant difference in the percentage of area flooded (∼6%). The inclusion of mean sea level variability (Figure 9, right) only contributes with ∼1% more of area flooded in both scenarios, consistently with the topography of the Ebro Delta. The percentage of area at risk of flooding for year 2099 increases substantially when extremes are accounted for, to a range between 83.6% and 90.5%.

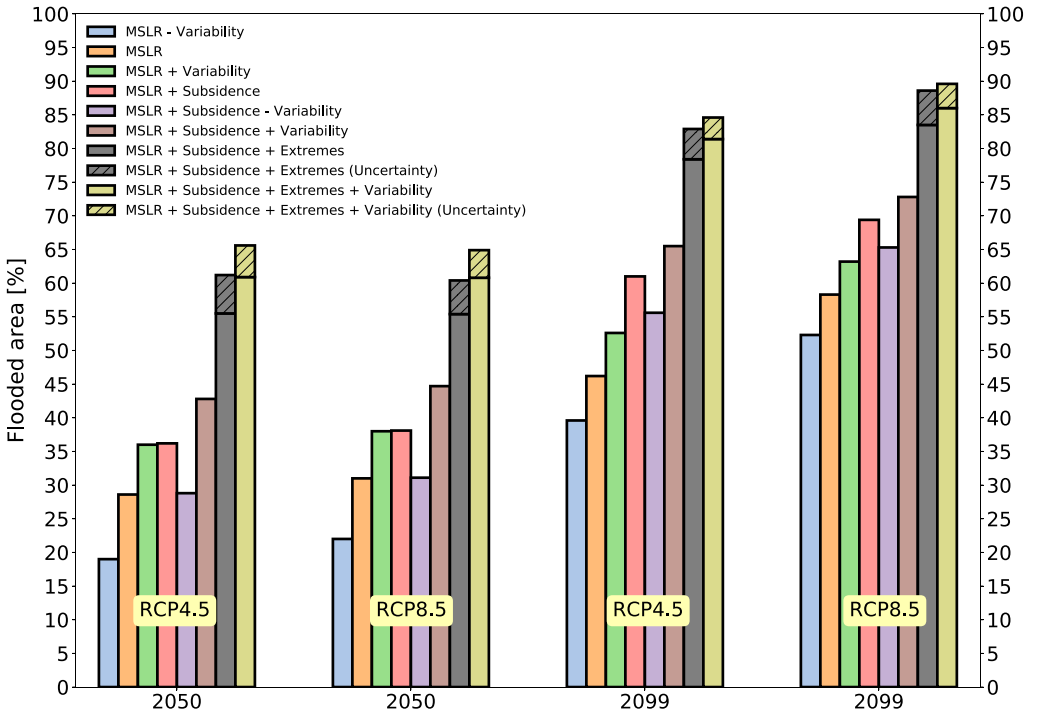

Figure 10. Ebro Delta percentage of area flooded (given in the range 0–100%) for scenarios RCP4.5 and RCP8.5 (indicated by yellow labels), and for years of interest 2050 and 2099. Each color corresponds to a different combination of factors: mean SLR, variability (seasonal and inter-annual signals), land subsidence and the combined effect of surge and waves extremes. Uncertainties from the different combinations of surges, H_s and T_p (percentile 99, percentile 50 and percentile 1) are indicated with hash lines.

5. Discussion and Conclusions

This study highlights the importance of all climate forcing terms that contribute to local relative sea level changes for coastal flood hazard risk analyses. In particular, the integration of seasonal and inter-annual mean sea level variability may enhance the impacts in coastal areas, since higher sea levels can be reached sooner than expected only from the response of mean SLR to increased radiative forcing. This is therefore a key factor to be considered in short to mid-term coastal planning (Nieves et al, 2017). Likewise, land subsidence may, in some areas, exacerbate the risks of mean SLR, as in the study case presented in this work which can be extended to most world deltas. Finally, the joint effect of extreme marine events must be considered when the probability of compound events exists. If extreme waves and surges are considered separately, the resulting risk assessment may be underestimated.

Our results in the western Mediterranean Sea regarding the joint probability distribution of surge and waves are in line with those discussed by Arns et al. (2017). They estimated changes in coastal design heights in the German Bight, a region with very different oceanic regime and where astronomical tides are important. Similarly to the method here presented, the joint effect of storm surges and waves was carefully analyzed with copula theory and projected inshore via run-up. However, the effect of seasonal and inter-annual variability and vertical land movements was not discussed at all. Therefore, this study intends to generalize the approach by including now these factors.

The impact of the different contributors to Ebro Delta flooding -in terms of percentage of the total flooded area- is summarized in Figure 10 for RCP4.5 and RCP8.5 scenarios. For instance, when considering only mean SLR and seasonal and inter-annual variability, the area at risk increases about 7% for year 2050 and 5% for year 2099 and for both scenarios (see the cases mean SLR-Variability and mean SLR + Variability, blue and green bars). In our particular case, the high rates of subsidence have a larger impact, increasing the flooded area by 6–7% for mid 21st century and for both scenarios (see mean SLR + Subsidence, pink bar), and near 15% for year 2099.

Because 50% of Ebro Delta is below 0.5 m over present-day mean sea level, some previous studies analyzed the effect of a relative sea level rise of this particular threshold (e.g., Sánchez-Arcilla et al., 1998, 2008) exploring the coastal response from a sediment balance standpoint. It is known that sediment distribution is important for horizontal and vertical accretion (Jiménez et al., 2017). Their results indicated a change in the morphology with a remarked coastal retreat of delta plain, with a redistribution of sediments toward the northern (mostly because of the dominant orientation of waves and longshore currents) and southern spits. In particular, in Sánchez-Arcilla et al. (2008) coastal risks were discussed from a climate change perspective by means of a sensitive analysis, changing arbitrarily some key drivers. They divided the inundated area by the degree of risk considering two levels: 1) areas below SLR directly connected with sea (prone areas); 2) other areas below SLR not directly connected with sea but with a coastal side that suffers strong erosion and breaching. For a relative SLR of 0.5 m the total area inundated adding the two levels of risk was 44% ((Sánchez-Arcilla et al., 2008), see Figure 5 therein). This magnitude is similar to the one shown here in Figure 5d, for year 2050 and RCP8.5 (44.7% for a relative SLR of 0.45 m, 0.35 of mean SLR and 0.1 m of subsidence). From their results they inferred that it is necessary at least four times more river water discharge to compensate sediment loss. However they did not address the effect of extremes due to the lack of climate projections of surges and waves at that moment.

IPCC scenarios from the Fourth Assessment Report (IPCC, 2007) were used in Alvarado-Aguilar et al. (2012) to investigate flood risk hazard in Ebro Delta. They considered a low, medium and high SLR scenarios and a range of subsidence rates, with an average value of 3 mm/year. Additionally, they analyzed the effect of manipulating channel connections and flood gates in Ebro Delta plain, concluding that for a relative SLR between 0.1 and 0.8 m, closing some critical points reduces flooded prone area about 60%. Otherwise for relative SLR higher than 0.9 m flooded prone area is only reduced 15%, and therefore they remark the need to find other alternatives. This relative SLR high scenario (0.9 m) is very similar to that obtained in this study in Figure 6c for a relative SLR of 0.92 m (mean SLR of 0.67 m and a subsidence of 0.25 m) for year 2099 and RCP8.5, with 69% of flooded area (61% for Alvarado-Aguilar et al., 2012, who consider regions directly connected with sea). Saltwater wetland, saline vegetation and riparian buffers will be the main affected zones, while urban areas are poorly impacted according to this study (Alvarado-Aguilar et al., 2012). More recently Genua-Olmedo et al. (2016) studied the effects of SLR on soil salinity of Ebro Delta and their impact on rice crops. To do this, they used RCP4.5 and RCP8.5 scenarios, mean and high SLR. However, in their model they only accounted for the global mean SLR, although it is well known that SLR is geographically nonuniform, and they did not include the effect of land subsidence as reliable measurements were still not available, or the contribution of sea flooding to delta surface loss. Their results, even with these shortcomings, concluded that salt intrusion will affect rice crops, with economic losses over 20% under the worst SLR high-end scenario of 1.8 m (Jackson & Jevrejeva, 2016).

Regarding the impact of extremes, the most energetic waves have an eastern origin and are usually accompanied by storm surges (Jiménez et al., 1997). Valdemoro et al. (2007) discussed storminess on Ebro Delta, indicating that the main effect is coastal flooding due to the absence of high enough barriers and dunes. Thus the degree of penetration of water inside land is related with the magnitude of swash and beach width. Jiménez et al. (1997) studied qualitatively the combined effect of storm surges and waves over Ebro Delta for an extreme event occurred in October 1990, with a water level of 0.75 mxeters and a significant wave height of 4.25 m. That event caused strong erosion on the coastline moving landward the backline, breaking barriers such as the connection between spits and delta plain and creating considerable breaches, connecting inland marshes and ponds with sea (Jiménez et al., 1997). In this study we have shown that surge and wave extremes increase substantially the flood risk with respect to MSL alone. As represented in Figure 10, extreme events contribute about 20% for RCP4.5 and RCP8.5 for years 2050 and 2099 (see mean SLR + Variability + Subsidence and mean SLR + Variability + Subsidence + Extremes, brown and kiwi bars). The range of uncertainties shown by the different combinations of extremes, derived from a range of possible water level s (see hash lines in Figure 10 and supporting information Figure S10) represent between 3 and 5% of the percentage of flooded area, which is of the order of mean SLR variability.

It must be recalled that our risk assessment does not contemplate any adaptation measure addressed to protect this vulnerable environment. Indeed, our results should be understood as an indication of the consequences of SLR and marine extremes if no actions are undertaken. The protection plan of Ebro Delta may consider the construction of dikes, which Genua-Olmedo et al. (2016) quantified in 1.5 m height. Other

studies have suggested solutions more in harmony with nature, such as to increase substantially river discharge of sediments, the protection of dunes and the creation of new ones (Fatorić & Chelleri, 2012). Also the increase of vegetation and adjust of marshes elevation to SLR can help dissipate energy, betting for an adaption more than for a protection. This philosophy is opposite to the most complete adaptation plans such as the Dutch National Adaptation Strategy and the Thames Estuary assessment (TE2100 Project), which focus mostly on reinforcing protection (Ibáñez et al., 2014). In any case, the strong anthropization of Ebro River basin and Ebro Delta raises the concern of the real scope of those solutions if they are not accompanied by a radical reduction of human pressure on Ebro River basin and by environmental governmental policies.

To conclude, one major constrain of this study focused on the Ebro Delta is that it has not considered erosion and redistribution of sediments. However, we believe the detailed and strict analyses of the climate forcing factors affecting the region will be a valuable tool and a first step toward an accurate evaluation of all the environmental, ecological and socio-economic impacts on the region. It is the necessary input, for example, to apply state-of-the-art complex sediment transport models to quantify sediment budget or to investigate changes in the land-use as well as modification in habitats of relevant species. In summary, the methodology developed in this work remains fully applicable to solve the impact of the combined effect of SLR and marine extremes at local scales, as far as regional simulations and long enough near in-situ data are available.

Acknowledgments

J.M. Sayol and M. Marcos thank financial support from CLIMPACT Project (CGL2014–54246-C2-1-R), funded by the Spanish Ministry of Economy and Competitiveness. Biel Jordà (IMEDEA), Samuel Somot (MeteoFrance) and Enrique Álvarez-Fanjul (Puertos del Estado) are acknowledged for providing regional simulations. Damià Gomis (Universitat de les Illes Balears) and Jordi Corbera (Institut Cartogràfic i Geològic de Catalunya) are acknowledged for providing Ebro Delta LIDAR data. Figure 7 and supporting information Figures S3–S5 have been plotted with MATLAB and Statistics Toolbox Release (2015b), The MathWorks, Inc., Natick, Massachusetts, United States. All other figures have been created with Python Software Foundation: numpy, matplotlib and scipy libraries. Python Language Reference, version 2.7. Available at http://www.python.org. Copula analysis has been performed with MATLAB toolboxes. A further description of methods and other complementary results are attached as supporting information in a separated file. The authors thank comments from two anonymous reviewers, which helped to improve substantially the original version of the manuscript.

References

Alvarado-Aguilar, D., Jiménez, J. A., & Nicholls, R. J. (2012). Flood hazard and damage assessment in the Ebro Delta (NW Mediterranean) to relative sea level rise. *Natural Hazards*, *62*, 1301–1321. https://doi.org/10.1007/s11069-012-0149-x

Arns, A., Dangendorf, S., Jensen, J., Talke, S., Bender, J., & Pattiaratchi, C. (2017). Sea-level rise induced amplification of coastal protection design heights. *Scientific Reports*, *7*, 40171. https://doi.org/10.1038/srep40171

Backhaus, J. O. (1985). A three-dimensional model for the simulation of shelf sea dynamics. *Deutsche Hydrographische Zeitschrift*, *38*(4), 165–187. https://doi.org/10.1007/BF02328975

Batstone, C., Lawless, M., Tawn, J., Horsburgh, K., Blackman, D., McMillan, A., et al. (2013). A UK best-practice approach for extreme sea-level analysis along complex topographic coastlines. *Ocean Engineering*, *71*, 28–39. https://doi.org/10.1016/j.oceaneng.2013.02.003

Brown, S., Nicholls, R. J., Hanson, S., Brundrit, G., Dearing, J. A., Dickson, M. E., et al. (2014). Shifting perspectives on coastal impacts and adaptation. *Nature Climate Change*, *4*, 752–755. https://doi.org/10.1038/nclimate2344

Carson, M., Köhl, A., Stammer, D., Slangen, A. B., Katsman, C. A., van de Wal, R. S., et al. (2016). Coastal sea level changes, observed and projected during the 20th and 21st century. *Climatic Change*, *134*(1), 269–281. https://doi.org/10.1007/s10584-015-1520-1

Church, J. A., Clark, P. U., Cazenave, A., Gregory, J. M., Jevrejeva, S., Levermann, A., et al. (2013). Sea level change. In T. F. Stocker et al. (Eds.), *Climate change 2013: The physical science basis*, *contribution of working group I to the fifth assessment report of the intergovernmental panel on climate change*. Cambridge, UK: CUP.

Coles, S. (2001). *An introduction to statistical modeling of extreme values*, *Springer series in statistics*. London, UK: Springer-Verlag.

Dangendorf, S., Marcos, M., Wöppelmann, G., Conrad, C. P., Frederikse, T., & Riva, R. (2017). Reassessment of 20th century global mean sea level rise. *Proceedings of the National Academy of Sciences of the United States of America*, *114*(23), 5946–5951. https://doi.org/10.1073/pnas.1616007114

Davison, A. C., & Smith, R. L. (1990). Models for exceedances over high thresholds. *Journal of the Royal Statistical Society, Series B: Statistical Methodology*, *52*(3), 393–442.

De Michele, C., & Salvadori, G. (2003). A Generalized Pareto intensity-duration model of storm rainfall exploiting 2-Copulas. *Journal of Geophysical Research: Atmosphere*, *108*(D2), 4067. https://doi.org/10.1029/2002JD002534

De Michele, C., Salvadori, G., Passoni, G., & Vezzoli, R. (2007). A multivariate model of sea storms using copulas. *Coastal Engineering*, *54*, 734–751. https://doi.org/10.1016/j.coastaleng.2007.05.007

Déqué, M., & Piedelievre, J. P. (1995). High resolution climate simulation over Europe. *Climate Dynamics*, *11*(6), 321–339. https://doi.org/10.1007/BF00215735

De Waal, D. J., & van Gelder, P. H. A. J. M. (2005). Modelling of extreme wave heights and periods through copulas. *Extremes*, *8*(4), 345–356. https://doi.org/10.1007/s10687-006-0006-y

Ebisuzaki, W. (1997). A method to estimate the statistical significance of a correlation when the data are serially correlated. *Journal of Physical Oceanography*, *10*(9), 2147–2153. https://doi.org/10.1175/1520-442(1997)010<2147:AMTETS>2.0.CO;2

Ericson, J. P., Vörösmarty, C. J., Dingman, S. L., Ward, L. G., & Meybeck, M. (2006). Effective sea-level rise and deltas: Causes of change and human dimension implications. *Global Planetary Changes*, *50*, 63–82. https://doi.org/10.1016/j.gloplacha.2005.07.004

Fatorić, S., & Chelleri, L. (2012). Vulnerability to the effects of climate change and adaptation: The case of the Spanish Ebro Delta. *Ocean & Coastal Management*, *60*, 1–10. https://doi.org/10.1016/j.ocecoaman.2011.12.015

Genua-Olmedo, A., Alcaraz, C., Caiola, N., & Ibáñez, C. (2016). Sea level rise impacts on rice production: The Ebro Delta as an example. *Science of the Total Environment*, *571*, 1200–1210. https://doi.org/10.1016/j.scitotenv.2016.07.136

Giosan, L., Syvitski, J., Constantinescu, S., & Day, J. (2014). Protect the world's deltas. *Nature*, *516*(7529), 31–33. https://doi.org/10.1038/516031a

Gringorten, I. I. (1963). A plotting rule for extreme probability paper. *Journal of Geophysical Research*, *68*, 813–814.

Hawkes, P. J., Gouldby, B. P., Tawn, J. A., & Owen, M. W. (2002). The joint probability of waves and water levels in coastal engineering design. *Journal of Hydraulic Research*, *40*(3), 241–251. https://doi.org/10.1080/00221680209499940

Holgate, S. J., Matthews, A., Woodworth, P. L., Rickards, L. J., Tamisiea, M. E., Bradshaw, E., et al. (2013). New data systems and products at the permanent service for mean sea level. *Journal of Coastal Research*, *29*(3), 493–504. https://doi.org/10.2112/JCOASTRES-D-12-00175.1

Ibáñez, C., Day, J. W., & Reyes, E. (2014). The response of deltas to sea-level rise: Natural mechanisms and management options to adapt to high-end scenarios. *Ecological Engineering*, *65*(4), 122–130. https://doi.org/10.1016/j.ecoleng.2013.08.002

IPCC (2007). Climate Change 2007: Impacts, adaptation and vulnerability. In *Contribution of working group II to the fourth assessment report of the intergovernmental panel on climate change*. Cambridge, UK: Cambridge University Press.

Jackson, L. P., & Jevrejeva, S. (2016). A probabilistic approach to 21st century regional sea-level projections using RCP and high-end scenarios. *Global Planetary Change*, *146*, 179–189. https://doi.org/10.1016/j.gloplacha.2016.10.006

Jiménez, J. A., & Sánchez-Arcilla, A. (1993). Medium-term coastal response at the Ebro delta, Spain. *Marine Geology*, *114*, 105–118.

Jiménez, J. A., Sánchez-Arcilla, A., Valdemoro, H. I., Gracia, V., & Nieto, F. (1997). Processes reshaping the Ebro delta. *Marine Geology*, *144*, 59–79. https://doi.org/10.1016/S0025-3227(97)00076-5

Jiménez, J. A., Valdemoro, H. I., Bosom, E., Sánchez-Arcilla, A., & Nicholls, R. J. (2017). Impacts of sea-level rise-induced erosion on the Catalan coast. *Regional Environmental Change*, *17*(2), 593–603. https://doi.org/10.1007/s10113-016-1052-x

Jordà, G., & Gomis, D. (2013). On the interpretation of the steric and mass components of sea level variability: The case of the Mediterranean basin. *Journal of Geophysical Research: Oceans*, *118*, 953–963. https://doi.org/10.1002/jgrc.20060

Jordà, G., Gomis, D., Álvarez-Fanjul, E., & Somot, S. (2012). Atmospheric contribution to Mediterranean and nearby Atlantic sea level variability under different climate change scenarios. *Global Planetary Change*, *80*, 198–214. https://doi.org/10.1016/j.gloplacha.2011.10.013

Kench, P. S., McLean, R. F., Brander, R. W., Nichol, S. L., Smithers, S. G., Ford, M. R., et al. (2006). Geological effects of tsunami on mid-ocean atoll islands: The Maldives before and after the Sumatran tsunami. *Geology*, *34*(3), 177–180. https://doi.org/10.1130/G21907.1

Kench, P. S., Thompson, D., Ford, M. R., Ogawa, H., & McLean, R. F. (2015). Coral islands defy sea-level rise over the past century: Records from a central Pacific atoll. *Geology*, *43*, 515–518. https://doi.org/10.1130/G36555.1

Kotz, S., & Nadarajah, S. (2000). *Extreme value distributions theory and applications*. Singapore: World Scientific.

Maldonado, A. (1972). El delta del Ebro. Estudio sedimentológico y estratigráfico, *Boletin de Estratigrafia*, *1*, 1–486.

Maldonado, A. (1986). Dinámica sedimentario y evolución litoral reciente del Delta del Ebro. In M. G. Marino (Ed.), *Sistema Integrado del Ebro* (pp. 33–B0). Madrid, Spain: Hermes.

Marcos, M., Jordà, G., & Cozannet, G. L. (2016). Sea-level rise and its impacts in the Mediterranean. In *The Mediterranean Region under climate change. A scientific update* (IRD éditions). Institut de Recherche pour le Développment.

Marcos, M., Jordà, G., Gomis, D., & Pérez, B. (2011). Changes in storm surges in southern Europe from a regional model under climate change scenarios. *Global Planetary Change*, *77*, 116–128. https://doi.org/10.1016/j.gloplacha.2011.04.002

Marcos, M., Tsimplis, M. N., & Shaw, A. G. P. (2009). Sea level extremes in southern Europe. *Journal of Geophysical Research: Oceans*, *114*, C01007. https://doi.org/10.1029/2008JC004912

Martínez-Asensio, A., Marcos, M., Jordà, G., & Gomis, D. (2013). Calibration of a new wind-wave hindcast in the Western Mediterranean. *Journal of Marine Systems*, *121–122*, 1–10. https://doi.org/10.1016/j.jmarsys.2013.04.006

Nelsen, R. B. (2006). *An introduction to copulas. Springer series in statistics*. New York, NY: Springer Science. ISBN-10: 0–387-28659-4.

Nicholls, R. J., & Cazenave, A. (2010). Sea-level rise and its impact on coastal zones. *Science*, *328*(5985), 1517–1520. https://doi.org/10.1126/science.1185782

Nieves, V., Marcos, M., & Willis, J. K. (2017). Upper-ocean contribution to short-term regional coastal sea level variability along the United States. *Journal of Climate*, *30*(6), 4037–4045. https://doi.org/10.1175/JCLI-D-16-0896.1

Ozga-Zielinski, B., Ciupak, M., Adamowski, J., Khalil, B., & Malard, J. (2016). Snow-melt flood frequency analysis by means of copula based 2D probability distributions for the Narew River in Poland. *Journal of Hydrology: Regional Studies*, *6*, 26–51. https://doi.org/10.1016/j.ejrh.2016.02.001

Pipia, L., Pérez, F., Marturià, J., Corbera, J., Jornet, L., & Rovira, A. (2016). Two decades of multi-sensor subsidence monitoring over Ebro Delta using coherence-based DInSAR techniques. In L. Ouwehand (Ed.), *Proceedings of living planet symposium 2016 (ESA SP-740)*. Prague, Czech Republic.

Reddy, M. J., & Ganguli, P. (2012). Bivariate flood frequency analysis of Upper Godavari River flows using Archimedean copulas. *Water Resource Management*, *26*(14), 3995–4018. https://doi.org/10.1007/s11269-012-0124-z

Rovira, A., & Ibáñez, C. (2007). Sediment management options for the lower Ebro River and its delta. *Journal of Soils and Sediments*, *7*, 285–295. https://doi.org/10.1065/jss2007.08.244

Rueda, A., Camus, P., Tomás, A., Vitousek, S., & Méndez, F. J. (2016). A multivariate extreme wave and storm surge climate emulator based on weather patterns. *Ocean Modelling*, *104*(8), 242–251. https://doi.org/10.1016/j.ocemod.2016.06.008

Ruti, P., Somot, S., Giorgi, F., Dubois, C., Flaounas, E., Obermann, A., et al. (2016). Med-CORDEX initiative for Mediterranean climate studies. *Bulletin of American Meteorological Society*, *97*(7), 1187–1208. https://doi.org/10.1175/BAMS-D-14-00176.1

Salvadori, G., De Michele, C., & Durante, F. (2011). On the return period and design in a multivariate framework. *Hydrology and Earth System Sciences*, *15*, 3293–3305. https://doi.org/10.5194/hess-15-3293-2011

Salvadori, G., Michele, C. D., Kottegoda, N. T., & Rosso, R. (2007). *Extremes in nature: An approach using Copulas. Water science and technology library 56*. Dordrecht, The Netherlands: Springer.

Sánchez-Arcilla, A., Jiménez, J. A., Stive, M. J. F., Ibáñez, C., Pratt, N., Day, J. W., Jr., & Capobianco, M. (1996). Impacts of sea-level rise on the Ebro Delta: A first approach. *Ocean & Coastal Management*, *30*(2–3), 197–216.

Sánchez-Arcilla, A., Jiménez, J. A., & Valdemoro, H. I. (1998). The Ebro Delta: Morphodynamics and vulnerability. *Journal of Coastal Research*, *14*(3), 754–772.

Sánchez-Arcilla, A., Jiménez, J. A., Valdemoro, H. I., & Gracia, V. (2008). Implications of climatic change on Spanish Mediterranean low-lying coasts: The Ebro Delta Case. *Journal of Coastal Research*, *24*(2), 306–316. https://doi.org/10.2112/07A-0005.1

Sánchez-Arcilla, A., Stive, M. F. J., Jiménez, J. A., & García, M. A. (1993). Impact of sea-level rise in a Mediterranean delta: The Ebro delta case, In *Seachange '93, Sea level changes and their consequences for hydrology and water management* (pp. IV53-IV62). Noord wijkerhout, the Netherlands: IHP/OHP.

Shiau, J. T. (2006). Fitting drought duration and severity with two-dimensional Copulas. *Water Resource Management*, *20*(5), 795–815. https://doi.org/10.1007/s11269-005-9008-9

Sklar, A. (1959). *Fonctions de répartition à n dimensions et leurs marges, 229–231*. Paris, France: Publications de l'Institut de Statistique de l'Université de Paris.

Slangen, A. B. A., Adloff, F., Jevrejeva, S., Leclerq, P. W., Marzeion, B., Wada, Y., & Winkelmann, R. (2017). A review of recent updates of sea-level projections at global and regional scales. *Survey in Geophysics*, *38*(1), 385–406. https://doi.org/10.1007/s10712-016-9374-2

Slangen, A. B. A., Carson, M., Katsman, C. A., van de Wal, R. S., Köhl, W. A., Vermeersen, L. L. A., & Stammer, D. (2014). Projecting twenty-first century regional sea-level changes. *Climatic Change*, *124*, 317–332. https://doi.org/10.1007/s10584-014-1080-9

Stockdon, H. F., Holman, R. A., Howd, P. A., & Sallenger, A. H., Jr. (2006). Empirical parameterization of setup, swash, and runup. *Coastal Engineering*, *53*, 573–588. https://doi.org/10.1016/j.coastaleng.2005.12.005

Syvitski, J. P. M., Kettner, A. J., Overeem, I., Hutton, E. W. H., Hannon, M. T., Brakenridge, G. R., et al. (2009). Sinking deltas due to human activities. *Nature Geoscience*, *6*, 681–686. https://doi.org/10.1038/ngeo629

Tessler, Z. D., Vörösmarty, C. J., Grossberg, M., Gladkova, I., Aizenman, H., Syvitski, J. P. M., & Foufoula-Georgiou, E. (2015). Profiling risk and sustainability in coastal deltas of the world. *Science*, *349*(6248), 638–643. https://doi.org/10.1126/science.aab3574

Tsimplis, M. N., Proctor, R., & Flather, R. A. (1995). A two-dimensional tidal model for the Mediterranean Sea. *Journal of Geophysical Research: Oceans*, *100*, 16223–16239. https://doi.org/10.1029/95JC01671

Valdemoro, H. I., Sánchez-Arcilla, A., & Jiménez, J. A. (2007). Coastal dynamics and wetlands stability. The Ebro delta case. *Hydrobiologia*, *577*, 17–29. https://doi.org/10.1007/s10750-006-0414-7

Van De Lageweg, W. I., & Slangen, A. B. A. (2017). Predicting dynamic coastal delta change in response to sea-level rise. *Journal of Marine Science and Engineering*, *5*(24), 1–12. https://doi.org/10.3390/jmse5020024

Wahl, T., & Chambers, D. P. (2014). Evidence for multidecadal variability in US extreme sea level records. *Journal of Geophysical Research: Oceans*, *120*, 1527–1544. https://doi.org/10.1002/2014JC010443

Wahl, T., Mudersbach, C., & Jensen, J. (2012). Assessing the hydrodynamic boundary conditions for risk analyses in coastal areas: A multivariate statistical approach based on Copula functions. *Natural Hazards and Earth System Sciences*, *12*, 495–510. https://doi.org/10.5194/nhess-12-495-2012

WAMDI Group (1988). The WAM model: A third generation ocean wave prediction model. *Journal of Physical Oceanography*, *18*, 1775–1810. https://doi.org/10.1175/1520-0485(1988)018<1775:TWMTGO>2.0.CO;2

Wöppelmann, G., & Marcos, M. (2016). Vertical land motion as a key to understanding sea level change and variability. *Review of Geophysics*, *54*, 64–92. https://doi.org/10.1002/2015RG000502